Inorganica Chimica Acta, 124 (1986) 101–114

PtL_3 X-ray Absorption Studies of Pt Model Compounds and $[(NH_3)_2Pt(OH)_2Pt(NH_3)_2]^{2+}$ Bound to DNA

A. P. HITCHCOCK, C. J. L. LOCK

Department of Chemistry and the Institute for Materials Research, McMaster University, Hamilton, Ont., L8S 4M1, Canada

and B. LIPPERT

Anorganisch-Chemische Institut der Technischen Universität Munchen, Lichtenbergstrasse 4, 8046 Garching, F.R.G.

(Received November 30, 1985)

Abstract

The Pt L_3 X-ray absorption spectra of a series of Pt compounds have been recorded and their extended fine structure (EXAFS) analysed to investigate the sensitivity of EXAFS to non-first-shell Pt–Pt distances. The Pt L_3 EXAFS spectra of complexes formed between $[(NH_3)_2Pt(OH)_2Pt(NH_3)_2]^{2+}$ and calf thymus DNA were also recorded. Pt–Pt vectors could not be detected in these spectra. When combined with the model compound studies, this result rules out Pt dimer structures for the Pt–DNA complex which involve rigidly bridged, adjacent Pt atoms. Such structures, based on dimeric bonding of a hydroxo dimer intermediate to DNA, have been proposed as models for cisplatin antitumor activity. These types of models now seem unlikely.

1. Introduction

cis-$Pt(NH_3)_2Cl_2$ cisplatin, (CS)* is a useful antitumor agent which is thought to operate through specific Pt–DNA interactions which inhibit DNA replication. Details of the mechanism of this interaction are not yet understood [1], but it is generally accepted that reaction of the platinum proceeds via a hydrolysis pathway with partial or complete solvolysis of the chloro ligands. Presently, the interaction of a monomolecular solvolysis species of cisplatin with two bases of DNA is favored, in particular with guanine [2]. However, there have been speculations on other reaction patterns (Fig. 1), for example that fixation of Pt to a guanine nucleobase might facilitate binding of a second Pt with the two metals relatively far removed from one another [3] (type **II**), or that two mononuclear nucleobase complexes

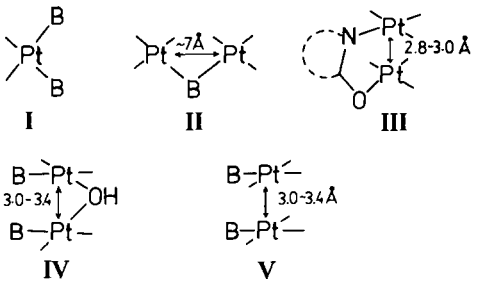

Fig. 1. Possible interactions of *cis*-Pt(II) with nucleobases B in DNA. (**I**) mononuclear complex, (**II**) nucleobase bridged complex (e.g. adenine N_7, N_1), (**III**) nucleobase bridged complex (e.g. guanine N_1, O_6 or thymine N_3, O_4), (**IV**) hydroxo bridged complex, (**V**) co-stacking of two mononuclear complexes.

condense to form a tight dinuclear arrangement, possibly through amidate bridges [4] (type **III**). The latter suggestion emerged from findings with uracil, thymine and related ligands where polynuclear, amidate bridged structures are readily formed [5–12]. Yet another feasible Pt–DNA interaction is that via hydroxo-bridged hydrolysis species of the type *cis*-$[(NH_3)_2Pt(OH)]_n^{n+}$ (n = 2,3) [1, 13–15] which might lead to dinuclear Pt complexes with the two metals bridged by a single OH bridge [16] (type **IV**). Finally, there is a possibility that two Pt atoms by accident might bind to two adjacent nucleobases without being connected with each other (Eichhorn co-stacking model) [17, 18] (type **V**).

It was the purpose of this study to use extended X-ray absorption fine structure (EXAFS) spectroscopy [19, 20] to investigate the possibilities of detecting Pt–Pt distances that might distinguish among the alternative Pt binding models outlined above. We have used EXAFS above the Pt L_3 edge to study the Pt environment in the complex formed by the reaction of the hydroxo-bridged Pt dimer cation, $[(NH_3)_2Pt(OH)_2Pt(NH_3)_2]^{2+}$ (DM) with calf

*Throughout this paper compounds are represented by a two letter code. The formulae of the compounds are summarized in Table I.

0020-1693/86/$3.50

TABLE I. Codes, Formulae, White Line Positions, Intensities and Coordination Charges for Platinum Compounds Studied

Code	Molecular formula[a]	Synthesis procedure and/or structure reference	White line position (±0.1 eV)	η[b]	m	White line intensity[c]
(a) Model compounds						
CS	*cis*-Pta_2Cl_2	41	+0.1	0.31	2	1.40
CY	$[a_2Pt(1\text{-MeC})_2](NO_3)_2\cdot(1\text{-MeC})$	47	+0.5(3)	0.29	2	1.34
DM	*cis*-$[a_2Pt(OH)]_2(NO_3)_2$	13	+0.5	0.26	2	1.38
DT	*cis*-$[a_2Pt(1\text{-MeT})]_2(NO_3)_2$ (head–head)	8, 12	+0.6(3)	0.26	2	1.54
HC	*cis*-$[a_2PtCl(CO_3)]_2$	48	+1.6(3)	0.32	3	1.99
HH	*cis*-$[a_2Pt(1\text{-MeU})]_2(NO_3)_2$ (head–head)	16	+0.5	0.26	2	1.38
HR	*cis*-$[a_2Pt(1\text{-Me}\cdot C\text{–}H)Cl]_2Cl_2$ (head–tail)	49	+2.0	0.31	3	1.95
HT	*cis*-$[a_2Pt(1\text{-MeU})]_2(NO_3)_2\cdot 3H_2O$ (head–tail)	7	+0.5	0.26	2	1.54
HU	$[(H_2O)a_2Pt(1\text{-MeU})_2Pta_2(NO_2)](NO_3)_3\cdot 5H_2O$ (head–tail)	45	+1.9	0.30	3	1.93
KC	K_2PtCl_4	42, 50	−0.4	0.35	2	1.43
KP	K_2PtCl_6	43, 50	+1.2	0.40	4	2.00
PE	$[Pt(en)_3]Cl_4$	50	+2.2(3)	0.28	4	2.20
PT	Pt metal	52	0	0	0	1.21
PV	*cis*-$a_2Pt(1\text{-MeU})Cl\cdot H_2O$	16	+0.4	0.29	2	1.37
PW	*cis*-$a_2Pt(1\text{-MeU})_2\cdot 4H_2O$	53	+0.7	0.26	2	1.52
TM	$[Pt(OH)(1,2\text{-dac})]_3(NO_3)_3$	40	+0.9	0.26	2	1.54
UH	*cis*-$[a_2(1\text{-MeU})Pt(OH)Pt(1\text{-MeU})a_2]ClO_4\cdot H_2O$	16	+0.6	0.26	2	1.49
XC	*cis*-Pta_2Cl_4	51	+1.5	0.36	4	1.86
XP	$a_2Pt(dien)Cl_3$	51	+1.9	0.34	4	2.35

Code	Complex	Pt:base ratio	Preparation		Relative white line position	White line intensity[c]
			T (°C)	Procedure		
(b) DNA preparations						
DF	DM + DNA	1:10	25	1-day rxn/2-wash	+0.5	1.39
DG	DM + DNA	1:10	0	1-day rxn/2-wash	+0.4	1.41
DH	DM + DNA	1:20	0	0.2-day rxn/1-wash	+0.4	1.31
DJ	DM + DNA	1:20	25	1-day rxn/2-wash	+0.5	1.43
DK	DM + DNA	1:20	0	1-day rxn/2-wash	+0.4	1.48
PN	DM + DNA	1:10	25	NO_3-buffer		1.45
PX	CS + DNA	1:10	25	NO_3-buffer	+0.7	1.40

[a]In the formulae given, a = NH_3, en = ethylene diamine, dien = diethanetriamine [$C_4N_3H_{14}$], 1,2-dac = 1,2-diaminocyclohexane, 1-MeU = 1-methyl uracil, 1-MeT = 1-methyl thymine, 1-MeC = 1-methyl cytosine and 1-MeC–H = deprotonated 1 methyl cytosine, and head–head (head–tail) refers to the relative orientation of the two nucleobase ligands. [b]Coordination charge $\eta = m(1 - \exp[(\chi_M - \chi_X)^2/4])$ where m = valence of Pt. Pauling electronegativity values as quoted in Cotton and Wilkinson [54] were used: Pt^{2+} = 2.28, Pt^{3+} = 2.40, Pt^{4+} = 2.50, Cl^- = 3.16, N = 3.04, O = 3.04. [c]Ratio of white line peak height to the Pt L_3 continuum jump after subtraction of a linear background through the L_3 continuum.

thymus DNA. In an earlier communication [21], we reported preliminary EXAFS data on this complex which gave evidence for a signal in the Fourier transform 'radial distance function' around 3 Å which was attributed to a Pt–Pt distance, indicating a type **III** (Fig. 1) dimeric binding mode. Subsequent, repeated studies have failed to reproduce this result. From our more recent and definitive work we conclude: (1) a Pt–Pt signal cannot be detected in the EXAFS of the DM–DNA complex, suggesting that most or all of the Pt–OH dimer dissociates during its interaction with DNA; and (2) the signal ascribed to Pt–Pt in the original report [21] arose either from unreacted Pt dimer (DM) or possibly was a noise artifact. The present paper is a complete report of our X-ray absorption studies on complexes of DM with calf thymus DNA and on a series of model compounds which investigate the Pt L_3 near-edge spectra and the sensitivity of EXAFS to various types of nonbonding Pt–Pt distances.

As radial distances get longer and the distance variability increases because of thermal motion or disorder, the ability of EXAFS to detect that distance decreases. Thus in order to evaluate our DM–

DNA results it was necessary to test the sensitivity of Pt L_3 EXAFS to Pt–Pt distances in different environments. This was achieved by studying a series of model compounds which included: dibridged Pt(III) species with two nucleobase bridges (HU, HR); a dibridged Pt(III) species with carbonato bridges (HC); nucleobase dibridged Pt(II) species without a direct Pt–Pt bond (DT, HH, HT); di and tri hydroxo-bridged Pt(II) species (DM, TM); a mono hydroxo-bridged Pt(II) species (UH); mononuclear Pt(II) complexes without bridging ligands (CS, CY, PW, PV); and Pt(II) and Pt(IV) chloride species (KC, KP, XC). The formulae for these species are given in Table I. To our knowledge the Pt L_3 EXAFS spectra of these species have not been reported previously. The Pt L_3 near edge spectra of K_2PtCl_4 and K_2PtCl_6 have recently been reported [22]. The structure of most of these compounds are known from X-ray crystallography (see Table I for refs.) although the structures of HC, TM, UH and PV have not been reported to our knowledge.

Previously, Teo *et al.* [23] have used Pt L_1 EXAFS to study the Pt environment in complexes formed by *cis*- and *trans*-$Pt(NH_3)_2Cl_2$ and calf-thymus DNA prepared under similar conditions and concentrations to the DM–DNA complexes studied in our work. They found no evidence for Pt–Pt interactions. Both chlorine ligands were lost on complexation and the derived nearest-neighbour distance and coordination number suggests that there are 4 N or O atoms in the first shell. Other recent EXAFS studies related to the present work include studies of Pt uridine blues and purples [24]; Pt-6-mercapto purine riboside complexes [25] and Rh carboxylate nucleobase clusters [26]. In addition, Wing *et al.* [27] have recently reported the first (low resolution) single crystal X-ray diffraction study of cisplatin binding to a short strand of DNA (a B–DNA dodecamer) showing exclusive binding at guanine N7. The Pt–N distance derived depended on the Pt loading due to shifts in the guanine position but the variation with Pt concentration suggested a normal Pt–N bond length around 2.0(1) Å.

The organisation of the paper is as follows. In section 2, the sample preparation, experimental procedures and data processing are described; in section 3 the Pt L_3 near edge spectra are discussed; in section 4, the Pt L_3 EXAFS of model compounds are used to illustrate the sensitivity of the technique to Pt–Pt distances in various environments; in section 5, the results of the DM–DMA complex studies are presented. Finally, in section 6, we discuss the significance of these results with regard to the mode of binding of Pt compounds to DNA and thus possible mechanisms of action of Pt antitumor agents such as cisplatin.

2. Experimental

2a. Sample Preparation

The model compounds used in this study were prepared according to published methods as indicated in the refs. in Table I. The DM–DNA samples were prepared as follows. A buffer solution of 10 mM $NaNO_3$ and 5 mM tris(tris(hydroxymethyl)aminomethane) was adjusted to pH 8.004 from about pH 9.7 with a few drops of 1 M HNO_3. 10 ml of this solution was added to an Erlenmeyer flask containing either 0.15 g or 0.3 g of freshly purchased calf-thymus DNA (Sigma Chemicals). It took a few minutes for all of the DNA to dissolve. An extra 0.5 ml of buffer was added to the flasks containing 0.3 g DNA. About 0.03 g of $[(NH_3)_2Pt(OH)]_2(NO_3)_2$ was added to each flask to give $Pt:PO_4^{3-}$ ratios of 1:20 and 1:10 based on an average nucleotide weight of 326. The mixtures were stirred overnight either on ice under a nitrogen stream or at room temperature in air. The mixtures were poured into 10 ml centrifuge tubes and ultracentrifuged at 57 000 rpm (~190 000 g) for 16.5 h. The supernatant was removed and the pellets were well stirred in fresh buffer solution (15 ml) and left in the refrigerator over the weekend. All solutions were then transferred to ultracentrifuge tubes and centrifuged for 16.5 h at 57 000 rpm. The clear pellets of DNA were transferred to small sample vials and dried under a nitrogen stream for 4 h and then under vacuum at room temperature for 2.5 h. The X-ray absorption spectra were recorded within 48 h after completing the preparation.

2b. Spectral Acquisition

The Pt L_3 X-ray absorption spectra were obtained with the C1 and C2 stations of the Cornell high energy synchrotron source [CHESS]. The C2 station employed a channel cut Si(220) monochromator while the C1 station used a double crystal monochromator. Harmonic rejection was accomplished by slightly misaligning the crystal orientation so that the intensity of the monochromator Bragg peak was reduced by 50%. The spectra were recorded in conventional transmission mode with a 10 cm long Ar filled (1 atm) ion chamber as monitor and a 30 cm long Ar ion chamber as detector. The spectra were recorded from 11.45 to 12.60 keV (sometimes to 13.20 keV) using either a constant 4 eV point spacing (290 points) or a more efficient, non-linear scan sequence of 10 eV/pt from 11.45–11.55 keV, 1 eV/pt from 11.55 to 11.60 keV, 4 eV/pt from 11.60–12.0 keV and 6 eV/pt from 12.0–12.6 keV (260 points). The energy scale was calibrated by assigning the value of 11 570.0 eV to the Pt L_3 white line of Pt metal. For accurate (±0.1 eV) measurements of edge shifts, edge spectra were recorded alternating between the compound of interest and a standard,

K_2PtCl_6 which was used because its white line (located at 11 571.2 eV) was among the sharpest of those studied.

The raw data in the form of accumulated detector signal for a given, constant monitor signal was stored on 8 inch floppy disks and subsequently analysed at McMaster. The detector signal was collected for periods of constant monitor signal rather than constant time to correct for variation in the incident photon flux. The normalizing signal was chosen so that the dwell time on each data point was between 1 and 2 seconds throughout the spectrum. In the 12 keV region studied the monochromated X-ray fluxes were *ca.* 10^{10} photons/eV/s for the circulating beam current and emittance angle used.

2c. Analysis

The raw spectra were converted to relative absorption by taking the negative logarithm of the detector counts. All EXAFS spectra for a particular compound at a particular temperature were then examined and those of high quality were summed. The spectra presented in the paper are generally the average of 2 to 6 single scans. The edge location was selected as the position of the half height of the edge jump which was within 2 eV of 11 564 eV in all cases. A multi-section, spline fit was then calculated and the size of the edge jump was used as a normalization factor. In most cases a fit with four equal cubic sections gave a suitable background function although a fit with four quadratic sections was better for these species which have only N or O first coordination shell signal and thus weaker and less rapidly varying EXAFS (CY, PW, TM). The spline background was subtracted from the data, the energy above the edge converted to a wavenumber scale [$k = (0.263(E - E_o))^{1/2}$, k in Å^{-1}, E in eV] and the data multiplied by a k^3 weighting factor to generate the EXAFS spectra as, $\chi(k)k^3 = k^3((\mu - \mu_o)/\mu_o)$.

The EXAFS spectrum was then truncated to establish k_{min} as the first node above 3 Å^{-1} and k_{max} as the highest value for which the signal clearly exceeded the noise (typically 14–16 Å^{-1}). The data were then interpolated to a constant k scale, zero-filled to 1024 channels and subjected to a fast Fourier transform. The magnitude of this transform is a phase-shifted radial distribution function. Accurate parameters were derived from isolated single shell structures by multiplying the R space data with a 1.0–1.5 Å wide window function centred on the peak of interest followed by reverse Fourier transformation to k-space. The Fourier filtered data were then divided into amplitude and phase components. The amplitude function gave information on the number of backscattering atoms (N), thermal motion (represented by a Debye–Waller type factor σ, the root mean square relative displacement along the interatomic distance) and the type of backscattering atom. The values of N and σ were obtained using the log ratio method [20], assuming a constant photoelectron mean free path in all materials. The radial distance, R, was obtained from the phase function ($2kR + \delta(k)$) by subtraction of a model phase function ($\delta(k)$) and correcting the k scales with a k-origin difference parameter (ΔE_o) chosen so that there was a zero intercept for the linear least-squares fit to the difference in the phase function of model and unknown. Both calculated [28] and experimentally-derived model phases were used.

For those cases where two distances were very similar and the transform peaks overlapped, the parameters (R, N, σ, ΔE_o) were obtained from a non-linear least-squares fit of the Fourier filtered multishell data to the single scattering EXAFS function:

$$\chi(k) = \sum_i \frac{N_i}{kR_i} A_i(k) e^{-2\sigma^2 i k^2} \sin[2kR_i + \delta_i(k)]$$

Again, model phase and amplitude functions were used to represent $A(k)$ and $\delta(k)$ for each component. Only relative Debye–Waller factors are obtained by EXAFS. These are very imprecise and difficult to make absolute even if single crystal X-ray scattering thermal motion factors are available since the degree of correlation in the motion is generally unknown. Thus we have not reported the derived Debye–Waller parameters and expect the derived coordination numbers to be of limited accuracy.

3. Pt L_3 Near Edge Spectra

The Pt L_3 spectra from 11.53 to 11.65 keV of a representative set (15 of 27) of the compounds studied are shown in Fig. 2. In each case a linear background following the continuum between 11.7 and 12.3 keV has been subtracted. Table I contains a summary of the positions of the $L_3 \rightarrow 5d$ 'white line' maxima relative to that of Pt metal, which was assigned a value of 11 570.0 eV. This edge feature dominates the Pt L_3 spectra in all compounds studied and always occurs within 2 eV of 11 570 eV. There are small but characteristic shifts in the white line position with oxidation state as would be expected if the d states are atomic like and more strongly affected by the net charge on the Pt atom rather than fine details of the local environment. Relative to Pt metal the L_3 white line is found 0.2 to 1.0 eV higher in Pt^{2+} compounds and 1.0 to 2.0 eV higher in Pt^{3+} or Pt^{4+} compounds. KC (K_2PtCl_4) has an anomalously low white line position, 0.4 eV below that of Pt metal. Our value for the white line position of KC (K_2PtCl_4) relative to KP (K_2PtCl_6) is −1.6(2) eV. This is in good agreement with the value of −1.8 eV measured from Fig. 4 of ref. 22. An earlier report by

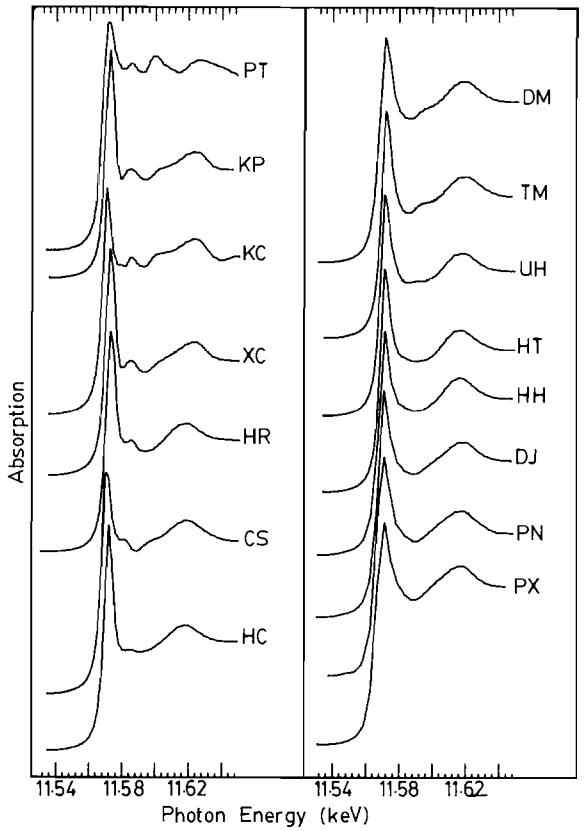

Fig. 2. X-ray absorption spectra of Pt compounds in the region of the Pt L_3 edge. PT, Pt metal; KP, K_2PtCl_6; KC, K_2PtCl_4; XC, $Pt(NH_3)_2Cl_4$; HR, *cis*-$[(NH_3)_2Pt(1\text{-}MeC\text{-}H)Cl]_2Cl_2$ (head-tail); CS, *cis*-$Pt(NH_3)_2Cl_2$; HC, *cis*-$[(NH_3)_2PtCl(CO)_3)]_2$; DM, $[(NH_3)_2Pt(OH)]_2(NO_3)_2$; TM, $[Pt(OH)(1,2\text{-dac})]_3(NO_3)_3$; UH, *cis*-$[(NH_3)_2(1\text{-}MeU)Pt(OH)Pt(1\text{-}MeU)(NH_3)_2]ClO_4 \cdot H_2O$; HT, *cis*$[(NH_3)_2Pt(1\text{-}MeU)]_2(NO_3)_2$ (head-tail); HH, *cis*-$[(NH_3)_2Pt(1\text{-}MeU)]_2(NO_3)_2$ (head-tail); DJ, DM + DNA complex (1:20, 0 °C rxn); PN, DM + DNA complex (1:10, 25 °C early result); PX, CS + DNA complex. Except for the uppermost spectrum of Pt metal, all of the spectra shown in the left hand panel, are of compounds which contain at least one Cl in the first coordination shell.

Padalia *et al.* [29] that the white line of K_2PtCl_6 is 10.5(5) eV above that of Pt metal is clearly wrong.

The intensity of the Pt L_3 white line is more sensitive, more reliably measured and more consistently characteristic of oxidation state than the white line position. Lytle *et al.* [30] have previously shown that the difference in L_3 white line area relative to Pt metal correlates well with the coordination charge η and thus, indirectly, to oxidation state ($\eta = mI$, where m = oxidation state, and the ionicity $I = 1 - \exp[-(\chi_M - \chi_x)^2/4]$). Horsley [31] showed that the sum of L_3 and half of the L_2 white line intensity can be used as a measure of d vacancy. We have explored the use of the white line intensity relative to the edge jump as a means of characterizing Pt compounds. These values are summarized in Table I along with the calculated coordination charge and formal oxidation state for each model compound. Strictly speaking the peak area relative to the area of a standard width of the continuum would be less sensitive to possible resolution changes or d-state splittings. However the observed peak widths are relatively similar in all cases (see Fig. 2) and thus the more easily measured peak height (relative to the continuum) was judged to be a reasonable estimate of the peak intensity. We find that this relative white line intensity parameter correlates well with oxidation state with values of 1.3–1.6 for Pt^{2+} compounds 1.8–2.0 for Pt^{3+} compounds and 1.9–2.4 for Pt^{4+} compounds. However, for this data set, the correlation between white line intensity and coordination charge suggested by Lytle *et al.* [30] was noticeably worse than the direct correlation of intensity with oxidation state.

A peak is observed at 11 585 eV in the spectrum of all 7 compounds examined which contain Pt–Cl bonds (6 of these are shown in the left-hand panel of Fig. 2). A corresponding feature can not be detected in the edge spectra of any Pt compound which does not have a Pt–Cl bond. This peak appears too sharp to be the first Pt–Cl EXAFS oscillation. It may be a σ shape resonance associated with multiple reflections of the L_3 ionized electron between the Pt and Cl atoms. Near-edge shape resonance features play a prominent role in the K-shell spectra of B, C, N, O and F containing species. The positions of σ resonances in light element K-shell spectra have recently been shown to correlate well with bond length and type of neighbouring atom [32]. Since the Pt–Cl bond length is very similar in all of the species studied, a σ(Pt–Cl) multiple scattering resonance would be expected to occur at the same location in all of the spectra. The association of this feature with Pt–Cl multiple scattering could be confirmed by polarization/orientation studies of a single crystal Pt–Cl compound as has been done with Cu–Cl resonances in Cu K spectra [33]. Regardless of the detailed assignment of this feature, the evidence presented in Fig. 2 indicates that a peak at 11 585 eV can be used as a characteristic fingerprint of Pt–Cl bonds. A similar approach has been used by Elder *et al.* [34] to identify phosphorus bonded to Au by the presence of a Au L_3 feature at 11 927 eV (about 8 eV above the Au L_3 edge). It is interesting to note that a Pd L_3 feature reminiscent of the Pt–Cl resonance is observed at 3179 eV (about 10 eV above the Pd L_3 edge) in $PdCl_2$ [35] but not in Pd compounds which do not contain Pd–Cl bonds.

With regard to characterising the Pt environment in the Pt–DNA complexes, comparison of the DM–DNA (DJ, PN) and CS–DNA (PX) L_3 edge spectra to those of the models clearly indicates that Pt is in the 2+ oxidation state (see the right hand panels of

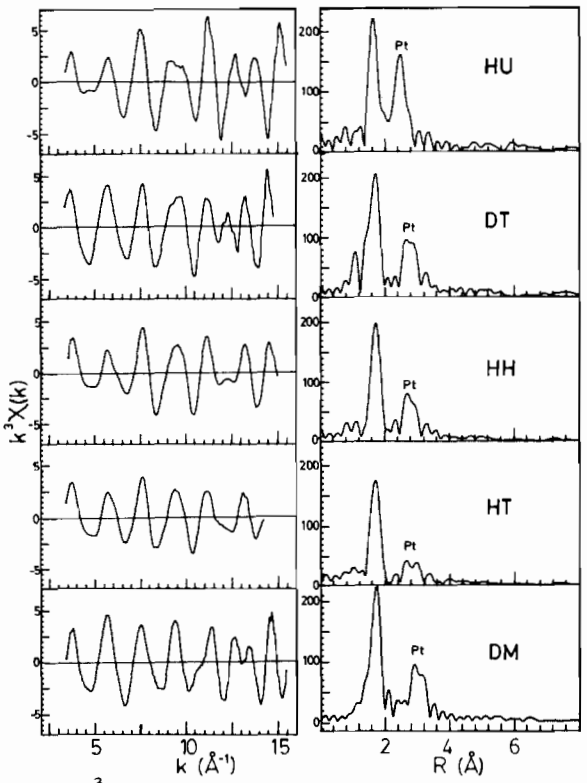

Fig. 3. k^3-weighted, Pt L_3 EXAFS (11.5–12.6 keV) (left-hand panels) and the Fourier transform, radial distribution functions (uncorrected for phase shifts) (right-hand panels) of: HU, $[(NO_2)(NH_3)_2Pt(1\text{-}MeU)_2Pt(NH_3)_2(OH_2)](NO_3)_3$ (head–tail); DT, $[(NH_3)_2Pt(1\text{-}MeT)]_2(NO_3)_2$ (head–head); HH, $[(NH_3)_2Pt(1\text{-}MeU)]_2(NO_3)_2$ (head–head); HT, $[(NH_3)_2Pt(1\text{-}MeU)]_2(NO_3)_2$ (head–tail) and DM, $[(NH_3)_2Pt(OH)]_2(NO_3)_2$.

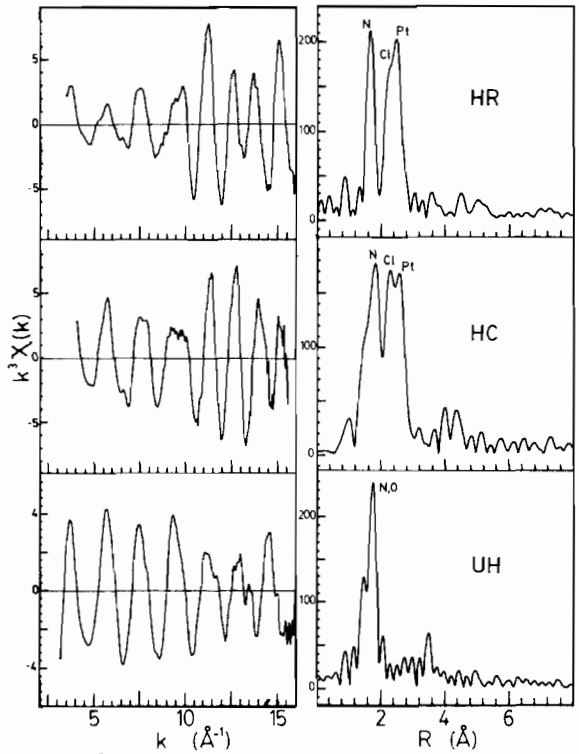

Fig. 4. k^3-weighted, Pt L_3 EXAFS (11.5–12.6 keV) (left-hand panels) and the Fourier transform, radial distribution functions (uncorrected for phase shifts) (right-hand panels) of: HR, $[(NH_3)_2Pt(1\text{-}Me\text{•}C\text{–}H)Cl]_2Cl_2$ (head–tail); HC, *cis*-$[(NH_3)_2PtCl(CO_3)]_2$; UH, *cis*-$[(NH_3)_2(1\text{-}MeU)Pt(OH)Pt(1\text{-}MeU)(NH_3)_2]ClO_4\text{•}H_2O$.

Fig. 2). The absence of a feature at 11 585 eV in the PX spectrum (CS–DNA) is evidence that the chlorides are lost in complexation of *cis*-$Pt(NH_3)_2Cl_2$ to DNA. This agrees with the conclusions drawn from the earlier L_1 [23] and present L_3 EXAFS results. This rules out any proposed Pt–DNA complex from cisplatin involving retention of Cl as a ligand.

4. EXAFS of Model Compounds

The normalized $k^3\chi(k)$ EXAFS and Fourier transform magnitudes derived from the Pt L_3 spectra of the model compounds are presented in 4 figs. Figure 3 presents the results for those species of known structure where the Pt–Pt distance is clearly detected. Fig. 4 presents the data for the species where the Pt signal overlaps that of another atom, Cl [HR, HC] or the Pt–Pt signal is detectable but very weak (UH), and Figs. 5 and 6 include the results for Pt metal and those species of known structure

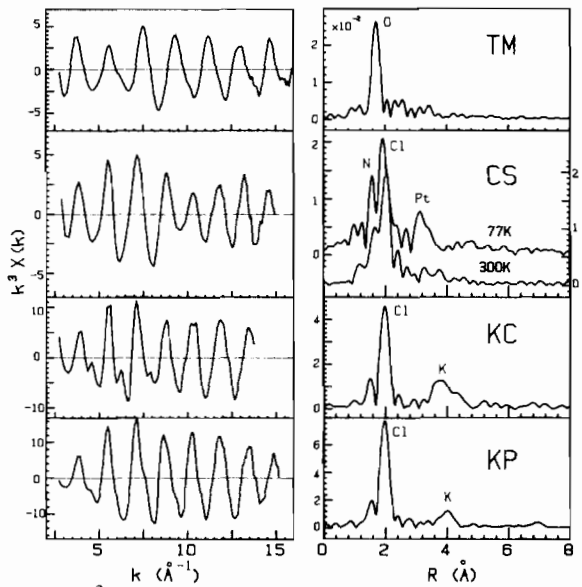

Fig. 5. k^3-weighted Pt L_3 EXAFS (11.5–12.6 keV) (left-hand panels) and the Fourier transform, radial distribution functions (uncorrected for phase shifts) (right-hand panels) for: TM, $[Pt(OH)(1,2\text{-}dac)]_3(NO_3)_3$; CS, *cis*-$Pt(NH_3)_2Cl_2$ (T = 300 K, lower; T = 77 K, upper); KC, K_2PtCl_4 and KP, K_2PtCl_6.

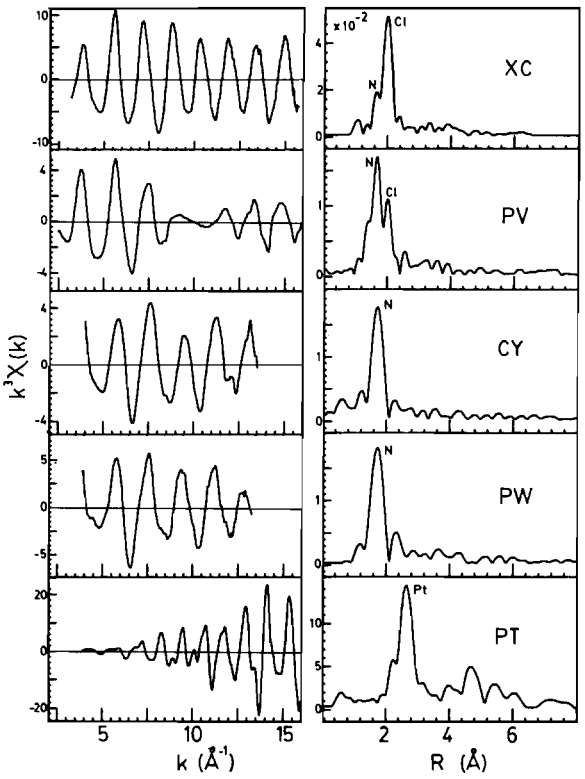

Fig. 6. k^3-weighted Pt L_3 EXAFS (11.5–12.6 keV) (left hand panels) and the Fourier transform, radial distribution functions (uncorrected for phase shifts) (right-hand panels) of: XC, $Pt(NH_3)_2Cl_4$; PV, *cis*-$(NH_3)_2Pt(1\text{-}MeU)Cl\cdot H_2O$; CY, *cis*-$[(NH_3)_2Pt(1\text{-}MeC)_2](NO_3)_2(1\text{-}MeC)$; PW, *cis*-$(NH_3)_2Pt(1\text{-}MeU)_2\cdot 4H_2O$ and PT, Pt metal.

where a Pt–Pt signal is not observed. Except for minor changes in the k-range transformed the data analysis procedures for the 18 spectra in Figs. 3–6 were identical and thus the vertical scales correctly reflect the relative intensities of various signals in the different compounds, k_{min} was between 3 and 4 Å^{-1} while k_{max} was between 13 and 17 Å^{-1}, depending on the strength of the EXAFS signal and data quality at high k. In all cases the k range transformed was greater than 9 Å^{-1}. As shown earlier with the Pt hydroxo dimer species [36], good quality data at high wavenumbers (above 12 Å^{-1}) is necessary to be able to detect non-nearest neighbour Pt–Pt distances since the Pt backscattering amplitude is greater at high k. All of the spectra shown in Figs. 3–6 were obtained at 77 K except that of CY (Fig. 6) which was recorded only at room temperature.

Table II summarizes the values for the Pt–Pt distances derived from the EXAFS of those species with a detectable Pt–Pt distance. In each case, the data was back-transformed (Fourier filtered) over the R range indicated in Table II. In most cases, the distance was then obtained from the phase function by correcting for the phase shift with calculated [28] and experimental models, choosing ΔE_o as the value which gave a zero intercept to the linearized phase difference function [20]. The experimental models included Pt metal PT, (Fig. 6), Pt hydroxo dimer (DM) and the Pt-base dibridge compounds of known structure which have a non-overlapping Pt–Pt signal (HU, DT, HH, HT). For HR and HC, where the Pt signal (R_{Pt-Pt} = 2.60 Å) overlaps with that from Cl backscattering [R_{Pt-Cl} = 2.43 Å], the value quoted in Table II was obtained by a two shell Pt, Cl fit to the Fourier filtered data. The results of the fits using Pt and K_2PtCl_4 model data are shown in Fig. 7 and the radial distance and coordination number parameters derived with a variety of models are summarized in Table III.

TABLE II. Pt–Pt Distances Derived from Pt L_3 EXAFS of Model Compounds

Species	EXAFS			Crystallography		
	$\Delta R_{transform}$[a]	R[b]	N[c]	R	N	Reference
HU	2.0–3.2	2.61(3)	1.5(1)[c]	2.574	1	45
DT	2.2–3.4	2.90(2)	1.0(1)	2.909	1	8, 12
HH	2.2–3.4	2.92(1)	1.2(2)	2.937	1	16
HT	2.2–3.4	2.93(1)	1.0(1)	2.954(2)	1	7
DM	2.4–3.5	3.12(1)	0.8(1)	3.085	1	13
CS	2.6–4.0	3.41(3)		3.37, 3.41	2	41
HR	1.8–3.2	2.60(1)[d]	0.8(1)[d]	2.60	1	49
HC	1.8–3.2	2.59(2)[d]	0.9(1)[d]			
UH	2.8–4.0	3.77(3)	1.9(3)			

[a]Range of R-space data back-transformed to k-space. The distance was then derived from the sine argument function by correction for phase shift effects using calculated [28] or experimental model phases and selection of a relative k-origin parameter (ΔE_o) by zero intercept of the linearized phase difference function [20]. [b]The errors quoted reflect both the degree of linearity of the phase difference function and the scatter in the results for different experimental models. [c]Based on the log ratio method [20] using DM data for the model amplitude (except for DM, where HH was the model). [d]From non-linear least-squares fits (see Table III).

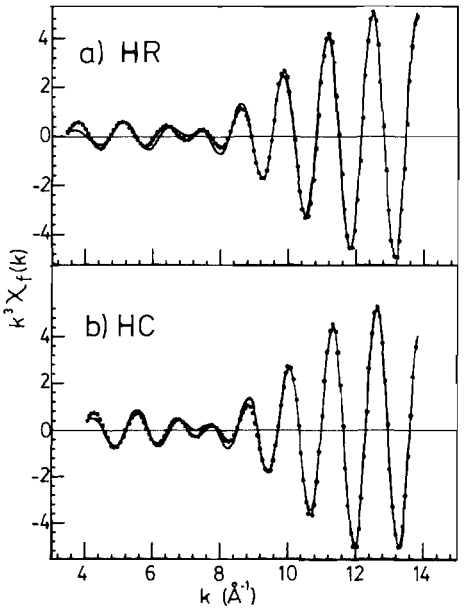

Fig. 7. Results of non-linear least-squares fits of two-shells (Pt, Cl) to Fourier filtered Pt L_3 EXAFS of (a) HR and (b) HC. The points are the Fourier filtered (1.80–3.20 Å) experimental data while the solid line is the calculated EXAFS based on the parameters obtained using K_2PtCl_4 and Pt metal data as model Pt–Cl and Pt–Pt phase and amplitude functions.

TABLE III. Results of Two-shell (Cl, Pt) Non-linear Least-squares Fits to HR and HC

Model	R_{Cl} (Å)	N_{Cl}	Model	R_{Pt} (Å)	N_{Pt}	$\Sigma\sigma^2$ [b]
(a) HR ($3.5 < k < 13.8$; $1.80 < R < 3.20$)[a]						
KP	2.450	0.7	PT	2.602	7.0	4.9
KC	2.438	0.6	PT	2.604	5.0	3.4
KP	2.483	0.3	HU	2.588	0.8	9.1
KC	2.472	0.3	HU	2.595	0.7	6.0
Average	2.46(2)	0.5(2)		2.60(1)	(3.0)	
Ref. 49	2.43	1		2.60	1	
(b) HC ($4.1 < k < 13.8$; $1.80 < R < 3.20$)[a]						
KP	2.483	0.3	HU	2.601	1.0	6.0
KC	2.472	0.3	HU	2.610	0.8	4.6
KC	2.492	1.0	DM	2.557	3.2	2.8
KC	2.455	0.8	PT	2.606	5.9	3.7
Average	2.48(2)	0.6(3)		2.59(2)	(3.7)	

[a]Range of Fourier filtered data upon which the fit was based and the R-space window used in the backtransform. [b]Quality of least squares fit.

At 77 K, we have assumed that there is a Gaussian distribution of Pt–Pt distances. If this is the case, there is a clear separation of the (ΔE_o, R) and (σ, N) EXAFS parameters and there should not be distortions in the derived distance, which sometimes arise with anharmonic systems. A potentially more serious limitation of our analysis is the assumption of a linear phase function. It is well known [28, 37] that the backscattering phase function for Pt is distinctly non-linear and thus a more sophisticated analysis for the phase shift would be desirable. However, we find good agreement between the Pt–Pt distances derived from EXAFS and those obtained from single crystal diffraction for the 6 compounds of known structure (average deviation is 0.02 Å). This suggests that the linearized phase difference analysis [20] is still applicable.

One further aspect to the determination of Pt–Pt distances in these types of systems is the possibility of multiple scattering effects. It is well known that backscattering from distant atoms can be greatly enhanced if there is an intervening atom. In such cases multiple scattering from this atom acts to focus and channel the outgoing and backscattered electron waves [38, 39]. This multiple scattering effect is greatest for systems which have linear bridges ($\theta = 180°$) and is generally considered to be negligible if the bridging angle, θ is less than 120°). Since the bridging angles are always less than 100° in the nucleoside and di or tri hydroxo bridged systems (e.g. $\theta_{Pt-O-Pt} = 81°$ in DM [13]) multiple scattering is not likely an important feature in these systems. One likely exception is UH where the experimentally derived Pt–Pt distance (3.77(3) Å) and the likely Pt–O distance (2.03 Å) imply a Pt–O–Pt angle of 138°. In this case multiple scattering is very likely enhancing the Pt backscattering. This probably explains why the Pt–Pt distance can be detected in UH but not in TM, the Pt hydroxo trimer. TM has a shorter Pt–Pt distance (3.39 Å) and probably a more rigid structure but the average Pt–O–Pt bond angle is only 110° [40] so that there is negligible multiple scattering enhancement.

Qualitatively the model compound results shown in Figs. 3–6 are of interest since they indicate the types of structures for which Pt–Pt distances can be determined by EXAFS. This is straightforward in directly bonded (HU, HR, HC) and dibridged (DT, HH, HT, DM) structures but becomes more difficult in monobridged structures (UH), those with very flexible bridged systems (TM which has a Pt–Pt distance of 3.39(3) Å [40]) or those structures where there are no covalently bonded linkages between Pt atoms (CS, KC, KP). The spectrum of cisplatin (CS) is of interest in this regard since this species has relatively short Pt–Pt distances (3.372 and 3.409(2) Å [41]) but there is no covalent bridging between adjacent platinums. The Pt–Pt distance cannot be detected by room temperature EXAFS but is clearly seen when the spectrum is recorded at liquid nitrogen temperature to a sufficiently high K range. Trans-

forms of 77 K and 300 K spectra of CS are shown in Fig. 5. This is presumably because of the large distance variation associated with uncorrelated thermal motion of two adjacent $[Pt(NH_3)_2Cl_2]$ molecules. The distance variation so broadens the Pt signal at room temperature that it does not form a distinct peak in the 3 to 3.5 Å region of the transform. The features around 4 Å in the transforms of K_2PtCl_4 (KC) and K_2PtCl_6 (KP) (Fig. 5) arise from backscattering by the K cations (at 4.2 [42] and 4.4 Å [43] respectively from Pt) rather than the more distant Pt atoms (at 4.6 to 4.7 Å). This was confirmed by the Fourier filtered amplitude function, which was characteristic of K rather than Pt, as well as the good agreement between the distance derived from EXAFS (R_{Pt-K} = 4.05(5) Å in KC and 4.35(10) Å in KP) and that from crystallography [42, 43].

In summary, it appears from these model compound studies that Pt–Pt distances can be detected most easily in structures with relatively rigid covalently bonded bridges such as those formed by the two hydroxyls in DM, the carbonates in HC, or the nucleobases in HU, DT, HH, HT, and HR. The insensitivity of EXAFS to distances between atoms which do not have constraints on their relative thermal motion has previously been noted [44]. Further discussion of the detection limits for Pt–Pt distances by EXAFS is given in section 5.

In addition to exploring the ability of Pt L_3 EXAFS to detect adjacent Pt atoms, the model compound spectra shown in Figs. 3–6 exhibit the well-known sensitivity of EXAFS to the first coordination shell. In those species in which the Pt is in a (roughly) square planar environment, bonded to 4 N or O atoms (HU, DT, HH, HT, DM, UH, TM, CY, PW), a single peak is observed in the transform spectra at 1.7 Å*. When the first coordination shell also contains Cl in addition to N (as in CS, XC, PV) additional signal is observed in the transform at 2.0 Å*. In HR and HC the Cl and Pt signals overlap strongly in the region between 2.0 and 2.8 Å*. In all cases, the relative intensities of the Cl and N signals reflect the relative numbers of Cl and N atoms in the first coordination shell of these species. Finally, when the first coordination shell contains only Cl (as in KC and KP) a single symmetric peak is observed at 2.0 Å* in the transform spectra.

The first shell distances and coordination numbers derived from the EXAFS analysis are summarized in Table IV. For those species with only a single type of atom in the first coordination shell the distances obtained from EXAFS agree with literature values within 0.03 Å and the coordination number is within 30% of the correct value. For species which have both N and Cl in the first coordination shell, the radial distances and coordination numbers reported in Table IV are the average of the values obtained from several curve fitting procedures using KC and KP as the model for the Pt–Cl phase and amplitude and HH as the Pt–N model. A summary of the Pt, Cl curve fitting results is given in Table V and examples of the quality of the fits are shown in Fig. 8. Where comparison to crystallographic values is possible, the Pt–N and Pt–Cl distances derived from the curve fitting procedures are generally found to be accurate. The coordination numbers obtained from curve fitting are significantly less accurate than those derived from single shell fits.

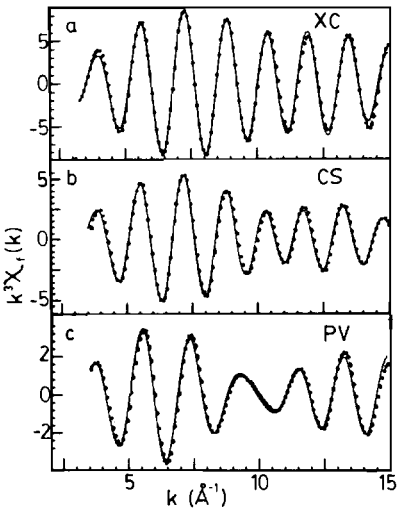

Fig. 8. Results of non-linear least-squares fits (solid line) of two-shells (N, Cl) to Fourier filtered Pt L_3 EXAFS (dots) of: (a) XC (3Cl, 1N), (b) CS (2Cl, 2N), and (c) PV (1Cl, 3N). The fitted curve was obtained using HH and KP for the Pt–N and Pt–Cl phase and amplitude functions.

5. EXAFS of Pt Hydroxy Dimer–DNA Complexes

The $k^3\chi(k)$ EXAFS and transform magnitudes of the Pt L_3 spectra of three of the 6 different preparations of $[(NH_3)_2Pt(OH)_2Pt(NH_3)_2]^{2+}$ (DM) and calf thymus DNA studied are shown in Fig. 9.

These preparations differ in the relative Pt:DNA base ratios and the temperature at which the reaction was carried out (DG–1 Pt: 10 bases, T = 0 °C, DJ–1 Pt: 20 bases, T = 25 °C; DK–1 Pt: 20 bases, T = 0 °C) but otherwise were prepared identically according to the procedure outlined in section 2a. It is clear from Fig. 9 that although there is weak signal in the 2.4–4 Å region of the transform, no distinct Pt–Pt vector is observed. Reverse transformation of the data between 2.8 and 3.8 Å gave amplitude functions peaking below 5 Å^{-1} (see Fig. 11d below), clearly

*These distances are uncorrected for phase shift effects and are listed only to aid spectral interpretation. See Tables III–V for the phase shift corrected values.

TABLE IV First Shell Distances and Coordination Numbers for Platinum Model Compounds and Pt–DNA Complexes

Species[a]	EXAFS		Literature values		
	R_1 (Å)[b]	N	R (Å)	N	Reference
(a) Model compounds: Pt–N or Pt–O distances					
CS	2.11(2)	3(1)	2.01(4)	2N	41
CY	2.02(1)	3.7(8)			47
DM	2.04(1)	3.4(1)	2.02(1)	2N, 2O	13
DT	2.03(1)	4.6(3)			8
HC	2.08(2)	4.7(3)			
HH	2.01(1)	4.7(2)	2.03(2)	3N, 1O	16
HR	2.01(2)	2.6(1)			
HT	2.02(1)	4.0(1)	2.05(2)	3N, 1O	7
HU	2.00(2)	3.9(1)	2.04(2), 2.253(9)	4N, 1O	45
PV[c]	2.02	1.3			
PW	2.05(2)	3.1(4)	2.048(7)	4N	53
TM	2.03(1)	4.1(4)	2.08(5), 2.11(3)	2O, 2N	40
UH	2.05(2)	4.0(4)			16
XC[c]	2.06	1.0			
Species	EXAFS		Literature values		
	R_{Cl} (Å)	N	R	N	Reference
(b) Model compounds: Pt- Cl distances					
CS[c]	2.34(1)	1.0(3)	2.33(1)	2	41
HC[d]	2.48(2)	0.6(3)		1	
HR[d]	2.46(2)	0.5(2)		1	49
KC	2.31(1)	3.5(3)	2.308(2)	4	42
KP	2.32(1)	6.8(4)	2.33	6	43
PV[c]	2.24	1.8(5)		1	
XC[c]	2.31	3.4(2)		3	
(c) DNA complexes					
DG	2.02(1)	4.1(2)			
DH	2.01(1)	5.0(3)			
DJ	2.02(1)	5.1(1)			
DK	2.03(1)	4.6(1)			
PN	2.04(1)	3.5(5)			
PX	1.99(2)	4.7(6)	2.03(1)	3.7(5)	23

[a]See Table I for molecular formulae. [b]HH (T = 77 K) data were used as the model phase shift for all Pt–N,O) distances (except HH where DM was used as the model). The error quoted reflects the degree of linearity of the phase function but does not include any systematic errors. [c]Values derived from a 2-shell curve fit (N, Cl) to filtered data (see Table V). [d]Values derived from a 2-shell curve fit (Cl, Pt) to filtered data (see Table III).

TABLE V. Results of Two-shell (N, Cl) Non-linear Least-squares Fits to Filtered Pt–L_3 EXAFS of *cis*-$Pt(NH_3)_2Cl_4$ (XC), *cis*-$Pt(NH_3)_2Cl_2$ (CS) and *cis*-$(NH_3)_2Pt(1\text{-MeU})Cl\cdot H_2O$ (PV)

Species	ΔR[a] (Å)	Nitrogen			Chlorine			$\Sigma\sigma^2$
		Model	R (Å)	N	Model	R_{Cl} (Å)	N_{Cl}	
XC	1.30–2.80	HH	2.06	1.3	KC	2.31	3.4	3.2
		HH	2.06	0.7	KP	2.31	3.5	2.6
CS	1.30–2.80	HH	2.09	1.6	KC	2.33	1.3	1.9
		HH	2.13	5.2	KP	2.35	0.7	2.4
PV	1.10–2.40	HH	2.02	1.4	KC	2.24	2.8	1.3
		HH	2.03	1.2	KP	2.24	3.2	1.5

[a]The results given are based on the fit to Fourier filtered data between 3.5 and 14.9 $Å^{-1}$.

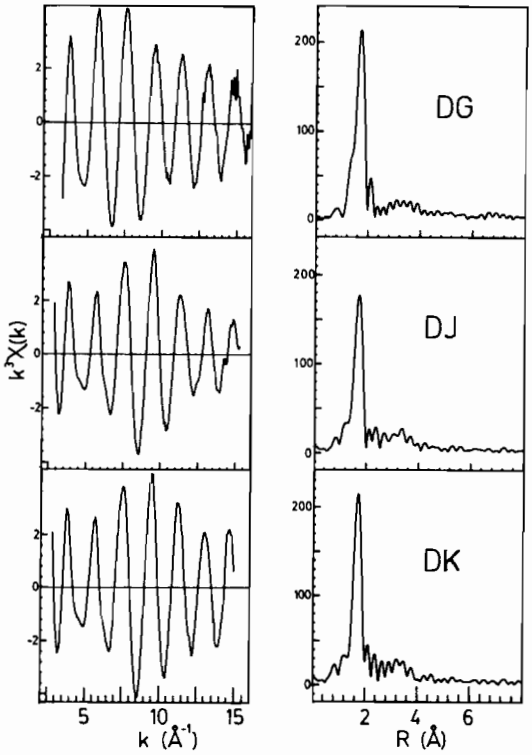

Fig. 9. k_3-weighted Pt L_3 EXAFS (11.5–12.6 keV) (left-hand panels) and the Fourier transform, radial distribution functions (uncorrected for phase shifts) (right-hand panels) of complexes formed between DM $[(NH_3)_2Pt(OH)]_2(NO_3)_2$ and calf-thymus DNA: DG, 1:10 Pt:base ratio reacted at 0 °C; DJ, 1:20 Pt:base ratio reacted at 25 °C; and DK, 1:20 Pt:base ratio reacted at 0 °C.

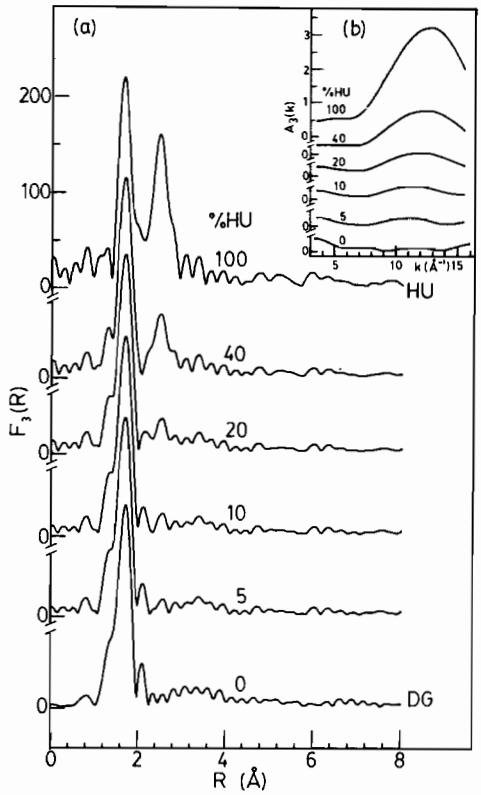

Fig. 10. Test of the sensitivity of Pt L_3 EXAFS to Pt–Pt distances. (a) Transform magnitudes of k^3 weighted EXAFS generated by summing the indicated percentage (x) of the HU spectrum along with a complementary component (100 – x) of the DG spectrum. All spectra are plotted on the same vertical scale with offsets for clarity. (b) The amplitude functions derived from back tranforming the spectra in (a) between 2.0 and 3.2 Å. Peaking of the amplitude shape above 10 Å^{-1} is indicative of a high-Z backscatterer. All spectra in (b) are plotted on the same vertical scale with the indicated offsets.

not that expected for Pt backscattering. We conclude that, within the detection limits of Pt L_3 EXAFS, there are no rigidly connected adjacent Pt atoms in our sample.

EXAFS spectra are the sum of signals from all environments of the core ionized atom. It is possible that there are a variety of Pt environments in the Pt-hydroxo dimer DNA complexes (DM–DNA). In order to investigate the ability of Pt L_3 EXAFS to detect Pt–Pt distances in mixed environments we have generated spectra by adding together varying proportions of the HU spectrum (the Pt complex with the most prominent Pt–Pt signal corresponding to a Pt–Pt distance of 2.574 Å [45]) and DG (a DM–DNA species, which does not exhibit a Pt backscattering signal). Figure 10 shows the radial distributions derived from the simulated EXAFS containing $x = 0.40$, 0.20, 0.10 and 0.05 HU and $(1 - x)$ DG. From these spectra a detection limit of about 20% is deduced. However, even for the spectrum containing only 5% HU signal the amplitude function derived from the backtransform of the 2.0 to 3.2 Å data peaks above 10 Å^{-1} (see the insert to Fig. 10). This indicates signal from a high Z backscatterer and, at least in this simulation, is direct evidence for a Pt backscatterer even though a clear peak can not be detected in the transform magnitude spectrum. This is a somewhat artificially favourable case for detecting Pt–Pt vectors in mixed environments since the Pt–Pt distance in HU is very short and thus the Pt signal is more distinct than in species with non-bonded but covalently bridged platinum atoms (HT, DM, DT). A realistic estimate of the detection limit might be 25% of environments with relatively rigid, covalently bridged platinum atoms. Thus our DM–DNA EXAFS results indicate that better than 75% of the Pt atoms are in environments which do not have covalent bridging to an adjacent Pt atom.

This conclusion is exactly the opposite to that which we reported earlier [21] based on preliminary studies. The difference could either be because the earlier result was a noise artifact or because there

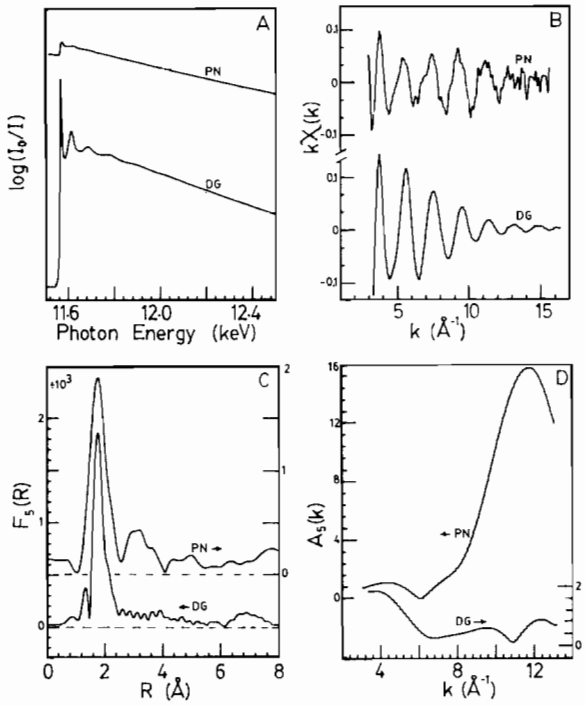

Fig. 11. Comparison of present (DG) and previous (PN) results for Pt hydroxo dimer DM–DNA EXAFS. (a) Pt L_3 absorption data (note that the ratio of edge jump to the negative slope of the continuum is a measure of the relative Pt content of the two samples); (b) isolated, normalized k^1-weighted EXAFS; (c) transform magnitudes obtained from k^5 weighted data to emphasize high k signal; and (d) amplitude functions of the components back transformed between 2.4 and 4.0 Å.

was a chemical difference between our first and subsequent DM–DNA samples. A detailed comparison of the present (DG) and earlier (PN) EXAFS results is present in Fig. 11. In earlier work, we have reported analysis of a high quality DM spectrum [36] over 5–10, 5–14 and 5–19 $Å^{-1}$ data ranges. This showed that good quality data above 10 $Å^{-1}$ is required to see clearly non-bonding Pt–Pt distances. However, the original DM–DNA spectrum (PN) was weak and thus quite noisy (Fig. 11a,b). From the raw absorption (Fig. 11a) it is clear that the Pt L_3 signal in the original preparation was much weaker, indicating a much lower degree of Pt uptake in this preparation. (Note that it is difficult to quantify the Pt concentration in our DM–DNA samples since the anisotropic DNA is very difficult to pack uniformly and thus the sample density is not well-known.) Largely as a consequence of the lower Pt L_3 intensity, the EXAFS isolated from the original spectrum is considerably noisier than the more recent results (Fig. 11b,c) and only a reduced data range (3–13 $Å^{-1}$) could be used. Even so, we think that the feature around 3 Å in the transform (Fig. 11c) of the earlier data (PN) is real, structurally-related signal and not solely noise. The reverse transforms of PN between 2.4 and 4.0 Å show an amplitude function (Fig. 11d) peaking around 11 $Å^{-1}$, indicating a high Z backscatter such as Pt, whereas the data filtered over the same region of any of the more recent DM–DNA spectra has an amplitude which peaks at low k indicating a low Z backscatter (probably C, N or O).

We suggest that for reasons not understood, there was less complex formed in the original preparation. Further, the washing procedure may not have been completely effective allowing some unreacted DM to remain in the sample. It is important to note that the conclusion we reach in this paper is based on much higher quality data and repeated analyses on different DM–DNA preparations.

The distances derived from the first shell signal of the DM–DNA complexes (Table IV) were obtained using the experimental first-shell DM data for the model phase function. The nearest-neighbour values are all within 0.02 of 2.02 Å. This is indistinguishable from the average Pt–N, O distance in DM [13] and the distance of 2.03(1) Å derived from Pt L_1 EXAFS of CS–DNA complexes [23]. Thus, there is not any measurable change of nearest neighbour distance upon formation of the DM–DNA complex or any significant difference from the first shell distance of CS–DNA. Since the Pt–N, O distances in all of the Pt-base model compounds are all similar (2.03 ± 0.04 Å) it seems that little specific information about the Pt binding site can be deduced from EXAFS determinations of the first shell data except to note that, by analogy with the Pt-base model compounds, the first shell distance is reasonable for a binding site at the heteroatoms of the nitrogenous bases. Similarly the imprecision of coordination number determination by EXAFS (see for example those derived for the model compounds, Table II) warrants caution in making any structural conclusions from the derived value of N for the DM–DNA complexes.

Discussion

The model compound studies show that when two platinum atoms are attached to one nucleobase in a fairly rigid arrangement Pt–Pt vectors of up to 3.4 Å are detectable. On this basis one can say from the EXAFS results that when $[Pt(NH_3)_2(OH)]_2^{2+}$ binds to DNA either it does not bind in the same way as is observed in model compounds [7, 12, 16] or, if such binding occurs, it is unstable and one or both of the platinum atoms migrate to other bases such that the platinum atoms are >3.4 Å apart. Thus the 'dimer model' for the anticancer activity of cisplatin [46] can be ruled out.

In the case of platinum atoms separated by 3.4 Å which are not rigidly bound together, our results

show that one cannot detect the Pt···Pt vector unambiguously. Thus it appears impossible to test the Eichhorn 'co-stacking model' [17, 18] by EXAFS. Nevertheless, such a model seems highly unlikely since the possibility of two platinum atoms being randomly bound to two adjacent bases *in vivo* is extremely low. Unless more positive evidence is available for a cooperative interaction this model should be discarded.

The absence of Pt–Pt signal in the EXAFS of the DM–DNA samples suggests that at least one and probably both of the OH bridges of the $[Pt(NH_3)_2(OH)]_2^{2+}$ break on complexation to DNA and are not replaced with short range covalent bridging by the nucleotides. Since a Pt–Pt vector was not observed in the flexible hydroxy trimer species, TM, we cannot rule out structures which contain a single OH bridge. However, this seems unlikely since oxygen is generally a poorer ligand to Pt than nitrogen and thus the basic nitrogen sites on the nucleobases might be expected to displace the hydroxyls.

Conclusion

Pt L_3 EXAFS of Pt–nucleobase model compounds has been studied to indicate the types of structures in which non-bonded Pt–Pt distances can be detected. The Pt L_3 EXAFS of the product of reaction between $[Pt(NH_3)_2(OH)]_2^{2+}$, DM, and calf thymus DNA does not exhibit a detectable Pt–Pt signal. Based on the model compound studies this rules out structures with rigid, covalent bridging and a Pt–Pt separation less than 3.4 Å. Models of cisplatin antitumor activity which invoke this type of dimeric binding can be ruled out.

Acknowledgements

We thank W. M. C. Pratt, M. L. Martins and M. Turner for preparing some of the model compounds and assisting in spectral recording. Financial support was provided by the Natural Sciences and Engineering Research Council of Canada (NSERC), the National Cancer Institute of Canada and Johnson, Matthey, Mallory Ltd. CHESS is a U.S. national facility supported by NSF. A. P. Hitchcock acknowledges financial support of an NSERC University Research Fellowship.

References

1 B. Rosenberg, *Biochimie, 60,* 859 (1978) and refs. therein.
2 M. P. Hacker, E. B. Douple and I. H. Krakoff (eds.), 'Platinum Coordination Complexes in Cancer Chemotherapy', Martinus Nijhoff, Boston, 1984.
3 A. D. Kelman, H. J. Peresie and P. J. Stone, *J. Clin. Hemat. Oncol., 7,* 440 (1977).
4 J. K. Barton and S. J. Lippard, *Ann. New York Acad. Sci., 313,* 686 (1979).
5 J. K. Barton, H. N. Rabinowitz, D. J. Szalda and S. J. Lippard, *J. Am. Chem. Soc., 99,* 2827 (1977).
6 J. K. Barton, D. J. Szalda, N. H. Rabinowitz, J. V. Waszczack and S. J. Lippard, *J. Am. Chem. Soc., 101,* 1434 (1979).
7 R. Faggiani, C. J. L. Lock, R. J. Pollock, B. Rosenberg and G. Turner, *Inorg. Chem. 20,* 804 (1981).
8 B. Lippert, D. Neugebauer and U. Schubert, *Inorg. Chim. Acta, 46,* L11 (1980).
9 C. J. L. Lock, H. J. Peresie, B. Rosenberg and G. Turner, *J. Am. Chem. Soc., 100,* 3371 (1978).
10 P. K. Mascharak, I. D. Williams and S. J. Lippard, *J. Am. Chem. Soc., 106,* 6428 (1984) and refs. therein.
11 R. Faggiani, B. Lippert, C. J. L. Lock and R. A. Speranzini, *J. Am. Chem. Soc., 103,* 1111 (1981).
12 H. Schoellhorn, U. Thewalt and B. Lippert, *Inorg. Chim. Acta, 93,* 19 (1984).
13 R. Faggiani, B. Lippert, C. J. L. Lock and B. Rosenberg, *J. Am. Chem. Soc., 99,* 777 (1977).
14 B. Lippert, C. J. L. Lock, B. Rosenberg and M. Zvagulis, *Inorg. Chem., 17,* 2971 (1978).
15 M. C. Lim and R. B. Martin, *J. Inorg. Nucl. Chem., 38,* 1911 (1978).
16 B. Lippert, D. Neugebauer and G. Raudaschl, *Inorg. Chim. Acta, 78,* 161 (1983).
17 R. C. Srivasta, J. Froehlich and G. L. Eichhorn, *Biochimie, 60,* 879 (1978).
18 C. J. L. Lock, R. A. Speranzini and M. Zvagulis, *Acta Crystallogr., Sect. B, 36,* 1789 (1980).
19 S. P. Cramer and K. O. Hodgson, *Prog. Inorg. Chem., 25,* 1 (1979).
20 P. A. Lee, P. H. Citrin, P. Eisenberger and B. Kincaid, *Rev. Mod. Phys.,* 53 (1981).
21 A. P. Hitchcock, C. J. L. Lock and W. M. C. Pratt, *Inorg. Chim. Acta, 66,* L45 (1982).
22 H. Terauchi, S. Iida, K. Tanabe, K. Kikukawa, H. Maeda, M. Hida and N. Kamijo, *J. Phys. Soc. Jpn., 52,* 3700 (1983).
23 B. K. Teo, P. Eisenberger, J. Reed, J. K. Barton and S. J. Lippard, *J. Am. Chem. Soc., 100,* 3225 (1978).
24 B. K. Teo, K. Kijima and R. Bau, *J. Am. Chem. Soc., 100,* 621 (1978).
25 M. A. Bruck, H. J. Korte, R. Bau, N. Hadjiliadis and B. K. Teo, *Am. Chem. Soc. Symp. Ser., 209,* 245 (1983).
26 N. Alberding, N. Farrell and E. D. Crozier, *J. Am. Chem. Soc., 107,* 384 (1985).
27 R. M. Wing, P. Pjura, H. R. Drew and R. E. Dickerson, *EMBO J., 3,* 1201 (1984).
28 B. K. Teo and P. A. Lee, *J. Am. Chem. Soc., 101,* 2815 (1979).
29 B. P. Padalia, S. N. Gupta and V. Krishnan, *Chem. Phys. Lett., 27,* 224 (1974).
30 F. W. Lytle, P. S. P. Wei, R. B. Greegor, G. H. Via and J. H. Sinfelt, *J. Chem. Phys., 70,* 4849 (1979).
31 J. A. Horsley, *J. Chem. Phys., 76,* 1451 (1982).
32 F. Sette, J. Stöhr and A. P. Hitchcock, *J. Chem. Phys., 81,* 4906 (1984).
33 S. Doniach, M. A. Berding, T. Smith and K. O. Hodgson, 'EXAFS and Near Edge Structure III', (Springer Proceedings in Physics 2), Springer, Berlin, 1984, p. 33; T. A. Smith, J. E. Penner-Hahn, K. O. Hodgson, M. A. Berding and S. Doniach, p. 58; N. Kosugi, T. Yokoyama, K. Asakura and H. Kuroda, *Chem. Phys., 91,* 249 (1984).
34 R. C. Elder, M. K. Eidsness, M. J. Heeg, K. G. Tepperman, C. F. Shaw and N. Schaeffer, *ACS Symposium Series, 209,* 385 (1983).

35 T. K. Sham, *Chem. Phys. Lett., 101,* 567 (1983); C. Sugiura and S. Muramatsu, *J. Chem. Phys., 82,* 2191 (1985).
36 A. P. Hitchcock, B. Lippert, C. J. L. Lock and W. M. C. Pratt, *Am. Chem. Soc. Symp. Ser., 209,* 209 (1983).
37 P. Rabe, G. Tolkiehn and A. Werner, *J. Phys. C., 12,* 899 (1979).
38 B. K. Teo, *J. Am. Chem. Soc., 103,* 3990 (1981).
39 N. Alberding and E. D. Crozier, *Phys. Rev. B, 27,* 3374 (1983).
40 P. Pilon, *Ph.D. Thesis,* McMaster University, Hamilton, Canada, 1984.
41 G. H. W. Milburn and M. R. Truter, *J. Chem. Soc. A,* 1609 (1966).
42 R. H. B. Mais, P. G. Owiston and A. M. Wood, *Acta Crystallogr., Sect. B, 28,* 393 (1972).
43 G. Engel, *Z. Kristallogr. A, 90,* 341 (1935).
44 S. P. Crawer, K. O. Hodgson, E. I. Stiefel and W. E. Newton, *J. Am. Chem. Soc., 100,* 2748 (1978).
45 B. Lippert, H. Schollhorn and U. Thewalt, *Z. Naturforsch., Teil B, 38,* 1441 (1983).
46 R. A. Speranzini, *Ph.D. Thesis,* McMaster University, Hamilton, Canada, 1980.
47 R. Faggiani, C. J. L. Lock and B. Lippert, *Inorg. Chem., 21,* 3210 (1982).
48 S. Jaworski and B. Lippert, to be published.
49 R. Faggiani, C. J. L. Lock and B. Lippert, unpublished.
50 R. N. Keller, *Inorg. Synth., 2,* 247 (1946).
51 D. C. Giedt and C. J. Nyman, *Inorg. Synth., 8,* 239 (1966).
52 H. J. Goldschmidt and T. Land, *J. Iron Steel Inst., 155,* 221 (1947).
53 D. Neugebauer and B. Lippert, *J. Am. Chem. Soc., 104,* 6596 (1982).
54 F. A. Cotton and G. Wilkinson, 'Advanced Inorganic Chemistry', 3rd edn., Interscience, New York, 1972, p. 115.